Letter

Enhancing fiber atom interferometer by in-fiber laser cooling

Yu Wang,[1] Shijie Chai,[1] Thomas Billotte,[2] Zilong Chen,[1] Mingjie Xin,[1] Wui Seng Leong,[1] Foued Amrani,[2] Benoit Debord,[2] Fetah Benabid,[2] and Shau-Yu Lan[1,*]

[1]*Division of Physics and Applied Physics, School of Physical and Mathematical Sciences, Nanyang Technological University, Singapore 637371, Singapore*

[2]*GPPMM Group, XLIM Institute, CNRS UMR 7252, University of Limoges, Limoges 87060, France*

(Received 20 December 2021; revised 7 February 2022; accepted 16 May 2022; published 13 June 2022)

We demonstrate an inertia sensitive atom interferometer optically guided inside a 22-cm-long negative curvature hollow-core photonic crystal fiber with an interferometer time of 20 ms. The result improves the previous fiber guided atom interferometer sensitivity by three orders of magnitude. The improvement arises from the realization of in-fiber Λ-enhanced gray molasses and delta-kick cooling to cool atoms from 32 μK to below 1 μK in 4 ms. The in-fiber cooling overcomes the inevitable heating during the atom loading process and allows a shallow guiding optical potential to minimize decoherence. Our results permit bringing atoms close to source fields for sensing and could lead to compact inertial quantum sensors with a submillimeter resolution.

DOI: 10.1103/PhysRevResearch.4.L022058

Quantum sensing deploys quantum phenomena to improve the sensitivity and stability of devices such as clocks, magnetometers, and accelerometers [1]. In particular, atom interferometric sensors commonly use optical pulses along atoms' trajectories to split, deflect and recombine two interferometer arms under quantum superposition. While large scale free space interferometers have shown unprecedented sensitivity in inertial sensing and test of fundamental physics [2–4], the apparatus that is used to house atoms typically has a cross section of tens of centimeters, set by the large laser beam sizes that are used to interact with atoms. Shrinking the apparatus size could lead to a compact device and allow the atoms to gain proximity to a source field of interest to enhance the signal, relaxing the stringent requirements in developing a portable sensor under dynamic environments.

In free space, reducing the laser beam waist comes at the cost of shortening the distance that atoms can effectively interact with the interferometer beams, thus decreasing the interferometer's sensitivity. Alternatively, hollow-core fibers offer a sub-millimeter enclosure that can guide the interferometer beams over diffraction free and configurable paths. However, most free space high sensitivity interferometers require preparation of ultra-cold atoms at sub-μK temperature in a low noise environment, and strategies to create such conditions for fiber atom interferometers remain to be developed.

For example, to guide a large number of atoms into a fiber and avoid their collision with the fiber wall, a deep trapping potential is necessary but generates inevitable heating on atoms during loading and guiding [5–9]. The large trapping potential also introduces decoherence on atoms' internal and external states through differential ac Stark shift and inhomogeneous dipole potential along the axial direction, limiting the fiber interferometer time to tens of μs [10]. Using only a few recoil energies of the trapping potential, atoms undergoing Bloch oscillations in an optical lattice have achieved 20 s of motional coherence time [11,12]. It is then necessary to cool atoms directly inside the fiber and lower the trapping potential to minimize the decoherence.

Unlike laser cooling in free space, the photonic structure of the fiber poses complications in cooling lasers' geometry and polarization. Although the cooling of atoms along the fiber axis has been demonstrated using sideband cooling [13], the scheme still requires a large trapping potential to confine atoms radially. Here, we implement gray molasses (GM) and delta-kick cooling (DKC), two commonly implemented cooling methods in free space atom interferometry, to cool the radial temperature of atoms inside the fiber.

We use an inhibited-coupling guiding hollow-core photonic crystal fiber (IC-HCPCF) with a tubular cladding made of eighttube singlering [14], as shown in Fig. 1. In contrast with capillary fibers, HCPCF is a true optical waveguide, ensuring very low loss and controllable modal content. As opposed to bandgap HCPCF, the core mode of IC-HCPCF is guided by decoupling the core and cladding modes. This is done by minimizing the spatial mode overlap and mismatching the effective indices between the core and cladding modes [14].

The fiber core has a diameter of 41 μm and the $1/e^2$ mode field diameter is 28.7 μm. It has losses of 8 dB/km at 780 nm and 18 dB/km at 1064 nm, which are suitable for trapping and probing Rb atoms. We mount a piece of 22-cm-long fiber vertically inside a vacuum chamber. Atoms are loaded from a two-dimensional magneto-optical trap (2D MOT) into a 3D MOT positioned 1.5 cm above the fiber. The temperature of

*sylan@ntu.edu.sg

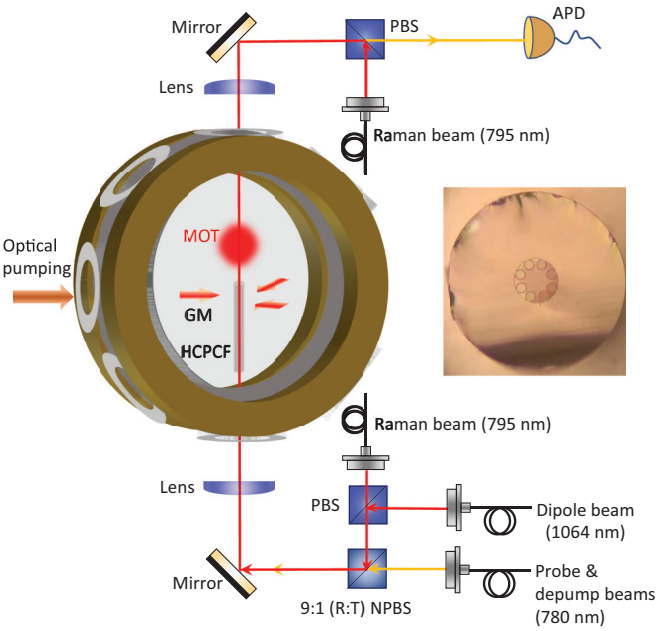

FIG. 1. Experimental setup. HCPCF: hollow-core photonic crystal fiber. PBS: polarization beamsplitter. NPBS: non-polarizing beamsplitter. GM: gray molasses beams. APD: avalanche photodetector. The 2D GM and optical pumping beam are aligned at 5 mm below the fiber tip. The inset shows the cross section of the fiber.

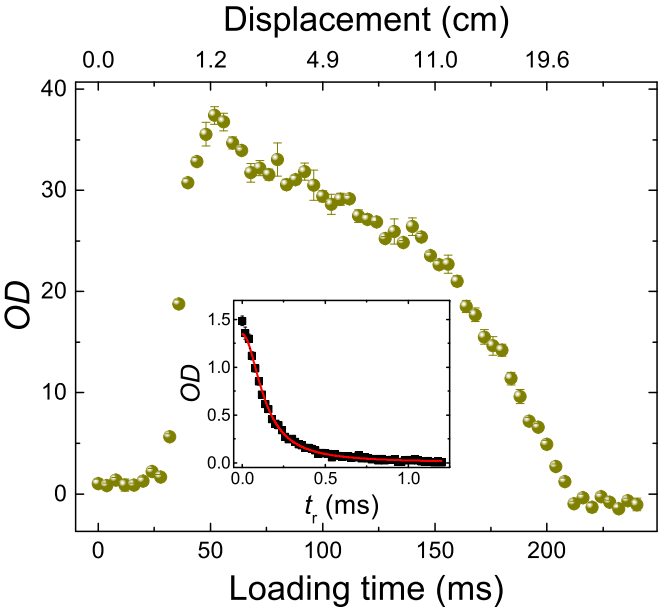

FIG. 2. *OD* versus loading time after releasing atoms from the MOT. The displacement axis is referenced to the MOT position and calculated using the value of the local gravity 9.78 m/s^2 under freefall. The inset shows time-of-flight measurements of atoms along the radial direction at 60 ms after loading, where t_r is the releasing time from the dipole trap.

the atoms after sub-Doppler cooling is 8 μK. After releasing atoms from the 3D MOT, gravity and a dipole force from a 700 mW 1064 nm laser attract them into the fiber.

The optical depth (*OD*) of atoms inside the fiber is determined by the transmission T_{tr} of a probe pulse as $OD = -\ln T_{tr}$. Fig. 2 shows the *OD* versus loading time and the position of atoms relative to the 3D MOT position. *OD* of one corresponds to approximately 6000 atoms in our experiment. The cloud begins to enter the fiber at 25 ms and fully exits the fiber at 210 ms. The cloud has a length of 3 mm at 40 ms measured by time-of-flight method. The major loss mechanism is due to the unwanted excitation of higher order modes and the fundamental mode forming a spatial modulation of the potential along the axial direction [8]. The increase of the atom loss rate after 150 ms is mainly due to a bend of the fiber where the dipole force is not strong enough to deflect atoms' trajectory.

We characterize the radial temperature of the atoms inside the fiber using the time-of-flight method [10,15]. We switch off the dipole beam and allow the cloud to expand ballistically for some time t_r. The probe pulse of 3 nW is then switched on for 50 μs for the *OD* measurement, as shown in the inset of Fig. 2. *OD* with different t_r can be calculated as

$$OD = \frac{OD_0}{2r^2/W^2 + 1} \tag{1}$$

where OD_0 is the optical density when $r = 0$, W is the $1/e^2$ radius of the guided mode, $r = \sqrt{r_0^2 + v^2 t_r^2}$ is the $1/e$ radius of the cloud at t_r, r_0 is the initial radius, $v = \sqrt{2k_B T_a/m}$ is the most probable speed of the atoms, T_a is the temperature of atoms, m is mass, and k_B is the Boltzmann constant. The initial radius of the cloud in the trap is related to the temperature as $r_0^2 = W^2 k_B T_a / 2U$, where U is the trapping potential. We fit Eq.(1) to the data and obtain the radial temperature $T_a = 32(1)$ μK. The increase of temperature is mainly due to the mismatch of the initial cloud and the dipole profiles.

After 60 ms of loading time, the cloud is 2.6 mm below the fiber tip, and we minimize the ambient magnetic field to tens of mG to implement a Λ-enhanced 2D GM. Λ-enhanced GM utilizes a Sisyphus cooling mechanism combined with coherent population trapping (CPT). CPT occurs in a three-level Λ-type system coupled to two coherent resonant light fields. Atoms in the bright state of CPT lose the kinetic energy by climbing up the optical potential from the light fields and are optically pumped into the dark state where atoms are decoupled from the light fields [16–18].

Our molasses lasers are comprised of three laser beams intersecting at 120° forming a plane perpendicular to the fiber, as shown in Fig. 1. This configuration allows for exciting the in-fiber atoms thanks to the negligible diffraction off the fiber microstructure. Each beam includes two frequencies which are +20 MHz detuned from ^{85}Rb D1 line $F = 2$ to $F' = 3$ and $F = 3$ to $F' = 3$ transitions, respectively. When these two frequencies are phase coherent, a dark-state formed by a superposition of $F = 2$ and $F = 3$ is created to enhance the cooling efficiency. The power ratio of the two frequencies is 35 to ensure all the atoms are accumulated in the $F = 2$ state after 3.2 ms of GM. Fig. 3(a) shows that the lowest temperature of 10 μK is achieved at two-photon resonance, a characteristic of GM involving the dark states from the Λ configuration. We observe a moderate increase of temperature 100 ms after GM to 35 μK.

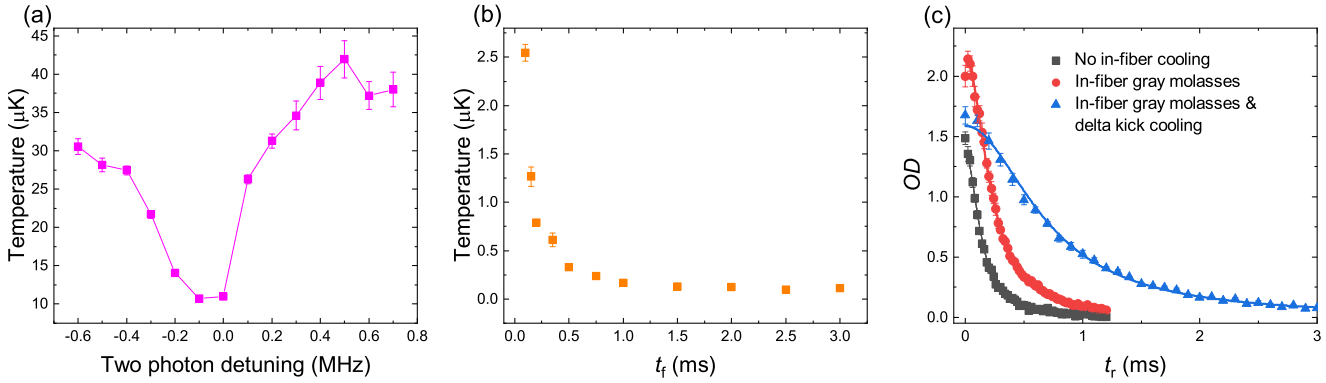

FIG. 3. (a) Measured temperature of atoms in the fiber after GM versus two photon detuning of the molasses beams. (b) Measured temperature after DKC with different free expansion time t_f. The kicking time t_k is determined by the lowest temperature. (c) A comparison of the time-of-flight measurements before and after GM and DKC. The fitted temperature for these three measurements are 32(1) μK (squares), 11.6(2) μK (circles), and 1.1(1) μK (triangles), respectively.

We minimize magnetic field decoherence by optically pumping atoms into $F = 2$ and $m_F = 0$ state [13]. We then perform DKC using the dipole trap. DKC involves pulsing a harmonic potential to halt the expansion of the cloud. Similar to adiabatic cooling, DKC trades the size of the ensemble for the temperature while preserving the phase space density. It has been widely implemented in atom interferometer experiments. We first switch off the dipole trap and let atoms expand for sometime t_f. This free expansion creates a correlation between the position and velocity of atoms, where atoms with higher velocity move farther away from the trap center. The trap is then switched on again for a duration of t_k and atoms are decelerated by the position dependent restoring force from the trap. The force stops the momentum of atoms under the condition $t_f t_k = 1/\omega^2$, where $\omega = 2\pi \times 3.7$ kHz is the radial trap frequency. The temperature T_a that can be achieved is determined by the free expansion time as $T_0/T_a = \omega^2 t_f^2$ when $\omega^2 t_f^2 \gg 1$, where T_0 is the initial temperature [19,20].

Fig. 3(b) shows the temperature measurements with different t_f, and t_k is determined by the best resultant temperature. At $t_f = 1$ ms, 165 nK is optimized at $t_k = 15$ μs. The lowest temperature starts to flatten out after $t_f = 1$ ms. This is mainly due to the anharmonicity of the trap. Moreover, due to the finite size of the guided mode, the long free expansion time for low temperature results in a significant atom loss. As shown in Fig. 3(c), the decrease of the temperature after GM also increases the density of atoms in the fiber by 30 %. At $t_f = 200$ μs and $t_k = 24$ μs, the fitted temperature of the time-of-flight measurements is 1.1(1) μK, a factor of two larger than the expected temperature of 0.5 μK. The product $t_f t_k = 4.8 \times 10^{-9}$ s^2 is a factor of three larger than $1/\omega^2 = 1.9 \times 10^{-9}$ s^2. These deviations from the ideal scenario also suggest the anharmonicity of the trap.

After the DCK pulse, we reduce the dipole power to 245 μW and start a Mach-Zehnder interferometer sequence (beamsplitter-mirror-beamsplitter) when atoms are under free-fall. The beamsplitter and mirror pulses are formed by a pair of counter-propagating laser beams driving a two-photon Raman transition on the $F = 2, m_F = 0$ and $F = 3, m_F = 0$ states, 20 GHz reddetuned from the $F = 2$ to $F' = 3$ states D1 line. The differential ac Stark shift from the dipole beam between these two states is estimated only 60 mHz. The mirror pulse duration of 1.5 μs corresponds to a two-photon Rabi frequency of $2\pi \times$ 333 kHz, larger than the measured Raman spectrum of 40 kHz of the velocity width of the atoms.

After the first interferometer beamsplitter pulse, the hyperfine states of atoms are entangled with their momentum states and thus the interferometer time is affected by the spin and motional coherence. The spin coherence of stationary atoms in the fiber has been demonstrated over 100 ms [21]. In this particular experiment, we measure the spin coherence of atoms under free-fall using spin echo sequence by a pair of copropagating Raman beams. The measured $1/e$ decay time of the spin echo contrast is 15 ms, limited by the inhomogeneity of the magnetic field. The relative momentum of the two arms of the interferometer is mainly influenced by the irregularity of the trapping beams during the interferometer sequence [22,23].

The phase at the output of the interferometer is $\phi = -k_{eff} a T^2 + \phi_1 - 2\phi_2 + \phi_3$, where a is the acceleration along the fiber axis, T is the separation time of the Raman pulses, and $\phi_{i=1,2,3}$ are the phases of the Raman pulses [10]. The population of atoms in the $F = 3$ state is $P = [1 - \cos(\phi)]/2$. We vary the phase ϕ_3 of the last Raman pulse and measure the population of atoms in the $F = 3$ state to scan the interference fringes. Each experimental cycle takes 1.8 s.

In Fig. 4(a), we observe two different decay trends of the contrast and fit the data with two exponentially decaying functions. The sharp decay of the contrast in the first 2 ms is due to radial expansion of the atoms in the shallow trap, which decreases the interferometer pulses efficiency. The inset shows the decay of the OD versus T and it matches well with the fast decay trend of the contrast. The second decay trend with fitted decaying constant of 7(3) ms is dominated by the phase fluctuation of the Raman beams from vibrations. To confirm that, we measure the linewidth of the beat note between the Raman beams to be 150 Hz after passing through the fiber, agreeing well with the contrast decay time we observe.

The highest acceleration sensitivity we obtain is 1.7×10^{-4} m/s^2 at $T = 5$ ms over 29 runs (1.2×10^{-3} m/s$^2/\sqrt{\text{Hz}}$), extending the previous fiber-based atom interferometer result 4 m/s$^2/\sqrt{\text{Hz}}$ [10] by three orders of magnitude. Our result is comparable with a fully guided Mach-Zehnder atom

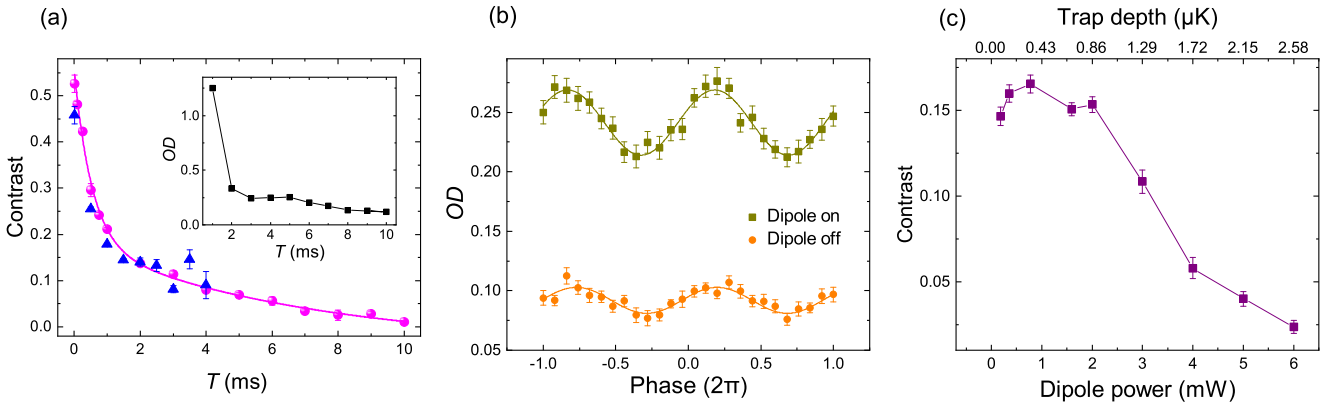

FIG. 4. (a) Contrast of the Mach-Zehnder interferometer versus pulse separation time T with dipole laser on (circles) and off (triangles) during the sequence. The curve is a fit to the dipole laser on data using sum of two decaying exponential functions. The inset is the mean of OD of the population in $F = 3$ state after the interferometer is closed versus T with dipole laser on. (b) Interference fringes with dipole laser on and off at $T = 3$ ms. The error bars are the standard error of the mean of 24 runs. (c) Contrast of the interference fringes versus different dipole laser power at $T = 2$ ms.

interferometer in free space of $7 \times 10^{-4}\,\mathrm{m/s^2}$ at $T = 1.25$ ms over 136 runs ($9\times10^{-2}\,\mathrm{m/s^2/\sqrt{Hz}}$) whose trap depth is similar to ours [24] and an unguided one of $5 \times 10^{-4}\,\mathrm{m/s^2}$ at $T = 3$ ms over 30 runs ($3\times10^{-2}\,\mathrm{m/s^2/\sqrt{Hz}}$) [24]. All the results are mainly limited by the path fluctuations of the interferometer beams.

The main improvement of our results from [10] is the colder atom temperature that allows us to use shallower trapping power to reduce the decoherence from the dipole force. To study the influence of the dipole laser only on the coherence, we perform measurements at short T when the dipole laser is off during the interferometer sequence. The dipole laser doesn't introduce additional decoherence at $T = 3$ ms but retains atoms in the trap, as shown in Fig. 4(a) and 4(b). In Fig. 4(c), the contrast at $T = 2$ ms starts to decrease at 2 mW of the dipole power due to the irregularity of the dipole beam along the fiber axis.

We expect to improve the initial contrast by three dimensional GM [25] and large bandwidth adiabatic rapid passage interferometer pulses [26,27]. A moderate improvement to $T = 50$ ms by installing a vibrational isolation platform can improve the sensitivity by two orders of magnitude. Improving the stability of atom loading and the atom number would improve the phase noise by another factor of 10, reaching $10^{-7}\,\mathrm{m/s^2}$. Such sensitivity can detect a ~1 kg nearby source mass distributed around the fiber while, for a free space atom interferometer with a 10 cm radius enclosure, two orders of magnitude higher sensitivity is required.

In summary, we demonstrate direct laser cooling of atoms inside a hollow-core fiber. The cooling schemes are also applicable to cold atoms trapped and guided by other photonic waveguides for quantum optics and many body physics experiments [28]. With colder atoms in the trap, we extend the coherence time of an inertia sensitive atom interferometer inside a hollow-core fiber to 20 ms with only 245 μW of the dipole beam and 10 μW of the Raman beams. The sub-millimeter package of the interferometer could allow short-range force and potential measurements with high spatial resolution and can find applications in constraining the deviation of Newton's law of gravity [29,30] and testing the quantum nature of gravity [31].

We thank M. Jaffe, C. Panda, and H. Müller for discussion. This work is supported by the Singapore NRF under Grant No. QEP-P4, the Singapore MOE under Grant No. MOE2018-T2-1-082, and H2020-FETOPEN-2018-2020 project CRYST3, Grant No. 964531.

[1] C. L. Degen, F. Reinhard, and P. Cappellaro, Quantum sensing, Rev. Mod. Phys. **89**, 035002 (2017).

[2] A. D. Cronin, J. Schmiedmayer, and D. E. Pritchard, Optics and interferometry with atoms and molecules, Rev. Mod. Phys. **81**, 1051 (2009).

[3] K. Bongs, M. Holynski, J. Vovrosh, P. Bouyer, G. Condon, E. Rasel, C. Schubert, W. P. Schleich, and A. Roura, Taking atom interferometric quantum sensors from the laboratory to real-world applications, Nat. Rev. Phys. **1**, 731 (2019).

[4] G. M. Tino, Testing gravity with cold atom interferometry: results and prospects, Quantum Sci. Technol. **6**, 024014 (2021).

[5] M. J. Renn, E. A. Donley, E. A. Cornell, C. E. Wieman, and D. Z. Anderson, Evanescent-wave guiding of atoms in hollow optical fibers, Phys. Rev. A **53**, R648 (1996).

[6] M. J. Renn, A. A. Zozulya, E. A. Donley, E. A. Cornell, and D. Z. Anderson, Optical-dipole-force fiber guiding and heating of atoms, Phys. Rev. A **55**, 3684 (1997).

[7] S. Okaba, T. Takano, F. Benabid, T. Bradley, L. Vincetti, Z. Maizelis, V. Yampol'skii, F. Nori, and H. Katori, LambDicke spectroscopy of atoms in a hollow-core photonic crystal fiber, Nat. Commun. **5**, 4096 (2014).

[8] Y. Wang, S. Chai, M. Xin, W. Seong Leong, Z. Chen, and S.-Y. Lan, Loading Dynamics of Cold Atoms into a Hollow-Core Photonic Crystal Fiber, Fibers **8**, 28 (2020).

[9] T. Peters, L. P. Yatsenko, and T. Halfmann, Loading and spatially resolved characterization of a cold atomic ensemble inside a hollow-core fiber, Phys. Rev. A **103**, 063302 (2021).

[10] M. Xin, W. S. Leong, Z. Chen, and S.-Y. Lan, An atom interferometer inside a hollow-core photonic crystal fiber, Sci. Adv. **4**, e1701723 (2018).

[11] N. Poli, F.-Y. Wang, M. G. Tarallo, A. Alberti, M. Prevedelli, and G. M. Tino, Precision Measurement of Gravity with Cold Atoms in an Optical Lattice and Comparison with a Classical Gravimeter, Phys. Rev. Lett. **106**, 038501 (2011).

[12] V. Xu, M. Jaffe, C. D. Panda, S. L. Kristensen, L. W. Clark, H. Müller, Probing gravity by holding atoms for 20 seconds, Science **366**, 745 (2019).

[13] Wui Seng Leong, M. Xin, Z. Chen, S. Chai, Y. Wang, and S.-Y. Lan, Large array of Schrödinger cat states facilitated by an optical waveguide, Nat. Commun. **11**, 5295 (2020).

[14] B. Debord, A. Amsanpally, M. Chafer, A. Baz, M. Maurel, J. M. Blondy, E. Hugonnot, F. Scol, L. Vincetti, F. Gérôme, and F. Benabid, Ultralow transmission loss in inhibited-coupling guiding hollow fibers, Optica **4**, 209 (2017).

[15] M. Bajcsy, S. Hofferberth, T. Peyronel, V. Balic, Q. Liang, A. S. Zibrov, V. Vuletić, and M. D. Lukin, Laser-cooled atoms inside a hollow-core photonic-crystal fiber, Phys. Rev. A **83**, 063830 (2011).

[16] D. Rio Fernandes, F. Sievers, N. Kretzschmar, S. Wu, C. Salomon, and F. Chevy, Sub-Doppler laser cooling of fermionic ^{40}K atoms in three-dimensional gray optical molasses, Europhys. Lett. **100**, 63001 (2012).

[17] Y.-F. Hsiao, Y.-J. Lin, and Y.-C. Chen, Λ-enhanced gray-molasses cooling of cesium atoms on the D2 line, Phys. Rev. A **98**, 033419 (2018), and references therein.

[18] L. Gabardos, S. Lepoutre, O. Gorceix, L. Vernac, and B. Laburthe-Tolra, Cooling all external degrees of freedom of optically trapped chromium atoms using gray molasses, Phys. Rev. A **99**, 023607 (2019), and references therein.

[19] T. Kovachy, J. M. Hogan, A. Sugarbaker, S. M. Dickerson, C. A. Donnelly, C. Overstreet, and M. A. Kasevich, Matter Wave Lensing to Picokelvin Temperatures, Phys. Rev. Lett. **114**, 143004 (2015).

[20] E. Maréchal, S. Guibal, J.-L. Bossennec, R. Barbé, J.-C. Keller, and O. Gorceix, Longitudinal focusing of an atomic cloud using pulsed magnetic forces, Phys. Rev. A **59**, 4636 (1999).

[21] M. Xin, W. S. Leong, Z. Chen, and S.-Y. Lan, Transporting Long-Lived Quantum Spin Coherence in a Photonic Crystal Fiber, Phys. Rev. Lett. **122**, 163901 (2019).

[22] R. Charrière, M. Cadoret, N. Zahzam, Y. Bidel, and A. Bresson, Local gravity measurement with the combination of atom interferometry and Bloch oscillations, Phys. Rev. A **85**, 013639 (2012).

[23] X. Zhang, R. Pablo del Aguila, T. Mazzoni, N. Poli, and G. M. Tino, Trapped-atom interferometer with ultracold Sr atoms, Phys. Rev. A **94**, 043608 (2016).

[24] G. D. McDonald, H. Keal, P. A. Altin, J. E. Debs, S. Bennetts, C. C. N. Kuhn, K. S. Hardman, M. T. Johnsson, J. D. Close, and N. P. Robins, Optically guided linear Mach-Zehnder atom interferometer, Phys. Rev. A **87**, 013632 (2013).

[25] S. Rosi, A. Burchianti, S. Conclave, D. S. Naik, G. Roati, C. Fort, and F. Minardi, Λ-enhanced grey molasses on the D2 transition of Rubidium-87 atoms, Sci. Rep. **8**, 1301 (2018).

[26] K. Kotru, D. L. Butts, J. M. Kinast, and R. E. Stoner, Large-Area Atom Interferometry with Frequency-Swept Raman Adiabatic Passage, Phys. Rev. Lett. **115**, 103001 (2015).

[27] M. Jaffe, V. Xu, P. Haslinger, H. Müller, and P. Hamilton, Efficient Adiabatic Spin-Dependent Kicks in an Atom Interferometer, Phys. Rev. Lett. **121**, 040402 (2018).

[28] D. E. Chang, J. S. Douglas, A. González-Tudela, C.-L. Hung, H. J. Kimble, Colloquium: quantum matter built from nanoscopic lattices of atoms and photons, Rev. Mod. Phys. **90**, 031002 (2018).

[29] F. Sorrentino, A. Alberti, G. Ferrari, V. V. Ivanov, N. Poli, M. Schioppo, and G. M. Tino, Quantum sensor for atom-surface interactions below 10 μm, Phys. Rev. A **79**, 013409 (2009).

[30] G. W. Biedermann, X. Wu, L. Deslauriers, S. Roy, C. Mahadeswaraswamy, and M. A. Kasevich, Testing gravity with cold-atom interferometers, Phys. Rev. A **91**, 033629 (2015).

[31] D. Carney, H. Müller, and J. M. Taylor, Using an Atom Interferometer to Infer Gravitational Entanglement Generation, PRX Quantum **2**, 030330 (2021).